17th World Conference on Nondestructive Testing, 25-28 Oct 2008, Shanghai, China

Mechanical characterization of porous structures by the combined use of micro-CT and in-situ loading

Greet KERCKHOFS.[1], Jan SCHROOTEN [1], Laida ELICEGUI [1], Simon VAN BAEL [2], Maarten MOESEN [1], Stepan V. LOMOV [1], Martine WEVERS [1]

[1]Department of Metallurgy and Materials Engineering, Katholieke Universiteit Leuven, B-3001 Leuven, Belgium, Phone: +32 16 321193, Fax: +32 16 321990; greet.kerckhofs@mtm.kuleuven.be, jan.schrooten@mtm.kuleuven.be, laida.elicegui@student.kuleuven.be, maarten.moesen@mtm.kuleuven.be, stepan.lomov@mtm.kuleuven.be, martine.wevers@mtm.kuleuven.be
[2]Department of Mechanical Engineering, Division of Production engineering, Machine design and Automation, Katholieke Universiteit Leuven, B-3001 Leuven, Belgium; simon.vanbael@mech.kuleuven.be

Abstract

To link the mechanical properties and failure mechanisms of porous materials to their morphology, the combination of micro-CT and in-situ loading was proposed as characterization technique. This approach allows to quantify the morphology prior and during loading. In this study, a newly designed micro-CT loading stage was validated against a standard mechanical testing device for porous Ti6Al4V structures produced by rapid prototyping with varying pore size and constant strut size. Also, the influence of stepwise loading on the global mechanical properties for these structures was assessed showing that indeed stepwise loading can introduce errors depending on the nature of the structure. Assessment of the morphology and mechanical properties showed no inter-batch variation per design, thus confirming the robustness of the production technique. Finally, stiffness and strength were correlated to the sample volume fraction and correlation functions can be used to tailor the design according to the required mechanical properties.

Keywords: porous structures, microfocus computed tomography, in-situ loading, mechanical properties

1. Introduction

In order to understand and simulate the behaviour of porous materials during mechanical loading, a thorough knowledge of the relationship between their morphology and mechanical behaviour on the one hand, and the failure mechanisms on the other hand is required. Since most commonly used methods to characterize porous materials are either empirical, indirect, often destructive, or not normalized and thus not suitable for a reliable comparison, the combined use of microfocus X-ray computed tomography (micro-CT) and in-situ mechanical loading is proposed as a characterization technique to unravel the previously mentioned relationships[1-13]. This approach allows (i) to quantify the morphology prior and during loading, (ii) to determine in situ the global mechanical properties, (iii) to analyze the failure mechanisms and (iv) to quantify the internal local strain distributions[14-17]. The information thus obtained enables to link the morphology to the mechanical properties and failure mechanisms, and can serve as input or validation for Finite Element (FE) modelling and robust design.

In this study, the mechanical behaviour of porous Ti6Al4V structures produced by rapid prototyping with varying pore size and constant strut size was investigated via the combination of micro-CT imaging and stepwise in-situ compression. First the accuracy of the developed micro-

CT loading stage was assessed by validation against a standard mechanical testing device. Then, the influence of stepwise loading with intermediate scanning on the global mechanical properties was investigated. Finally, the inter-batch variation of the morphology and mechanical properties was determined to check the robustness of the production technique, followed by a correlation between the morphology and the mechanical properties.

2. Materials and methods

2.1 Materials

Three different batches (n = 15) of cylindrical porous Ti6Al4V samples with regular structure and with varying pore and constant strut size were investigated (figure 1a). Table 1 summarizes their design parameters. They were produced by rapid prototyping (RP) and more specific by selective laser melting (SLM)[18, 19]. RP techniques[20-22] allow the production of porous materials that are based on a robust computer design, thus allowing a high morphological property control and hence eventually a wider use. All cylinders had a radius of 3.00 ± 0.05 mm and a height of 12.0 ± 0.5 mm. The design made use of unit cells, which can also be applied for FE modelling and determination of local surface strains as shown in figure 1b.

2.2 Micro-CT equipment

A detailed description of micro-CT can be found in Ref.[23-25]. For this study, a Philips HOMX 161 X-ray system with AEA Tomohawk CT software was used. Characteristics of the device and the applied acquisition parameters can be found in Ref.[26]. In this study the thickness, width and height of the image voxels were 13.9 µm.

2.3 Mechanical loading devices

A mechanical loading stage was developed which can be installed inside a micro-CT device for in-situ measurements. This loading stage has the following advantages against others found in literature: (i) high forces can be attained (up to 30kN), (ii) monitoring and control of relaxation is possible, (iii) no tubing is present around the sample, thus low density polymers can be visualised accurately and (iv) there is a possibility to add a cooling/heating or an oxygen- and/or moisture-level regulated chamber. For standard mechanical testing, an INSTRON universal test bench, type 4505 equipped with an extensometer was used as reference. The compression rate was kept approximately the same on both loading devices, namely 0.15mm/min. On the INSTRON, a load cell of 5kN was used while the load cell on the micro-CT loading stage was 30kN.

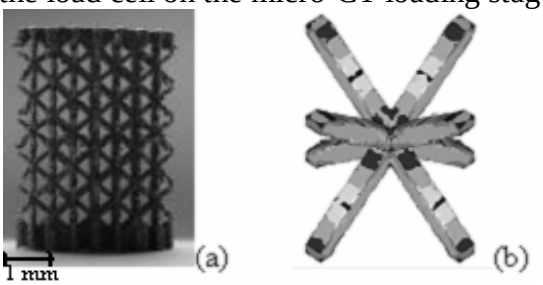

Figure 1. a) A typical cylindrical porous Ti6Al4V structure with a radius of 3.00 ± 0.05 mm, a height of 12.0 ± 0.5 mm and a global porosity of about 85 %. Designed pore size is 0.8 mm.
(b) A typical unit cell of the designed porous structures. The differing grey values on the struts represent the surface strains under certain loading conditions.

Table. 1. Design parameters for the three different batches.

Batch	**Designed pore size (mm)**	**Designed strut size (mm)**	**n**
1	0.800	0.100	15
2	1.000	0.100	15
3	1.200	0.100	15

3. Results and discussion

To determine whether the difference between paired groups was significant, a student t-test was performed.

3.1 Validation of the micro-CT loading stage versus a standard mechanical testing device

Validation of the micro-CT loading stage against a standard mechanical testing device was performed on all three batches. Five samples per batch were continuously loaded on the INSTRON and five on the micro-CT loading stage. A typical stress-strain curve is shown in figure 2. Since the designed porous structure shows non-linear elastic properties, the stiffness is defined as the maximum of the derivative of the stress-strain curve. Table 3 summarizes the results for stiffness, compressive strength and strain at maximum load. There was no significant difference between the results. This indicated that the micro-CT loading stage renders accurate and correct global mechanical properties.

3.2 Influence of stepwise loading

In literature[8, 9] it was reported that there should be no significant difference between the mechanical properties derived from continuous or stepwise loading. In this study, the goal was to determine whether this statement could be confirmed for the developed micro-CT load stage and the assessed samples. Apart from continuous loading, samples were tested during stepwise loading with intermediate micro-CT imaging. First, a preload of 10N was applied. Then, the compression test was stopped every 0.2 mm of displacement until first failure occurred. Figure 2 shows a typical stress-strain curve of which the shape is representative for all three batches. It can be seen that during imaging a drop in the load occurred which is caused by the rotation of the sample. Table 4 shows the stiffness, compressive strength and strain at maximum load determined on the micro-CT loading stage during stepwise loading. In contrast to what has been reported in literature[8, 9], there is indeed a significant difference between the results from table 3 and 4 when the stiffness and strain at maximum load are concerned. Strength values show no significant difference. However, it should be mentioned that, when the stiffness would be determined by the slope of the first data points in the stress-strain curve (in the linear elastic region), the difference might not be significantly different. This will be assessed in further research.

3.3 Micro-CT image analysis and correlation with the mechanical properties

The combination of mechanical testing and micro-CT imaging allows to determine the morphological properties of each sample prior and during stepwise loading. In this way, a correlation can be made between the morphological and the mechanical properties. The analysed morphological properties based on the micro-CT datasets of all samples preloaded at 10N are summarized in table 5 together with physically measured properties.

Table 3. Stiffness, compressive strength and strain at maximum load determined both on the INSTRON and the micro-CT loading stage for five samples per batch.

	E-modulus (MPa)		**Strength (MPa)**		**Strain at maximum load (%)**	
Batch (n = 10)	**INSTRON**	**Micro-CT loading stage**	**INSTRON**	**Micro-CT loading stage**	**INSTRON**	**Micro-CT loading stage**
1	389.68 ± 22.64	369.76 ± 29.83	15.70 ± 0.30	14.81 ± 1.41	9.2 ± 0.5	7.3 ± 0.4
2	225.56 ± 20.46	237.74 ± 16.40	8.05 ± 0.28	8.04 ± 0.22	7.3 ± 0.2	7.2 ± 0.4
3	79.93 ± 5.15	81.89 ± 4.92	3.97 ± 0.09	3.87 ± 0.22	9.0 ± 0.6	8.2 ± 0.2

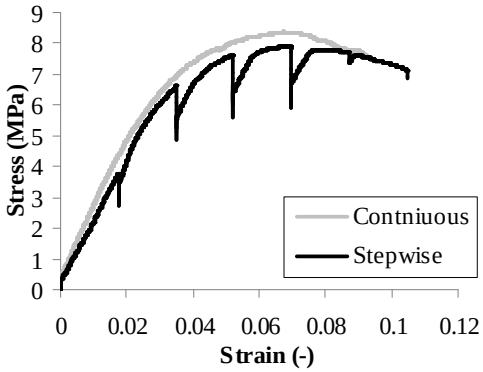

Figure 2. Typical stress-strain curves of a continuously and a stepwise loaded sample with the same design. For each imaging step, a drop in the load is noticed.

It can be seen that the micro-CT based porosity values correspond well to those determined via the Archimedes principle, which serves as a physical reference[27, 28]. A small underestimation of the porosity is seen, which is mainly caused by the partial volume effect[26, 29, 30]. Table 5 also indicates that for each morphological parameter, the standard deviation within one batch is small. The same is seen in table 3 for the mechanical properties. This confirms the robustness of the production technique. Moreover, it indicates that one random sample within a batch is sufficient for a full batch characterization.

Additionally, table 5 confirms that the main difference between the three batches is the pore size and consequently also the specific surface and the porosity. It should be mentioned that the pore size in table 5 is an average value. In reality however, a distribution of pores with different diameter was found, which can be seen in figure 3A. The designed pore size and the one derived from the micro-CT data are defined differently and hence cannot be directly compared. For the struts also a distribution in diameter was found which was equal for the three batches. In figure 3B, two peaks can be distinguished. The second peak, at larger strut size, represents the nodes in the unit cell (fig. 2b) and hence should not be accounted for as a strut. Therefore, a Gaussian curve was fitted to the first peak and the mean of this curve was taken as the average strut size of the structures. For the three batches, an average strut size of 178 ± 44 µm was found. Since the structures assessed in this study were designed close to the physical production limits, a difference between design (100 µm) and reality (178 µm) was expected.

Table 4. Average and standard deviation of stiffness, compressive strength and strain at maximum load determined on the micro-CT loading stage for five samples per batch during stepwise loading.

Batch (n = 5)	**E-modulus (MPa)**	**Strength (MPa)**	**Strain at maximum load (%)**
1	481.77 ± 28.12	14.49 ± 0.95	7.2 ± 0.7
2	267.03 ± 28.81	7.78 ± 0.18	6.5 ± 0.1
3	108.17 ± 8.22	3.69 ± 0.13	7.7 ± 0.6

Table 5. Morphological parameters derived via the Archimedes principle and from the micro-CT data via image analysis for the three different batches.

	Archimedes	**Micro-CT**				
Batch (n=5)	**Porosity (%)**	**Porosity (%)**	**Specific surface (1/mm)**	**Anisotropy**	**Avg. Pore size (µm)**	**Avg. Strut size (µm)**
1	85.28 ± 0.49	80.52 ± 1.08	21.94 ± 0.65	0.59 ± 0.02	480 ± 8	187 ± 5
2	88.13 ± 0.10	85.43 ± 0.33	21.59 ± 0.63	0.61 ± 0.02	601 ± 4	187 ± 4
3	92.24 ± 0.15	90.71 ± 1.14	22.75 ± 0.67	0.68 ± 0.10	776 ± 12	181 ± 5

Finally, as shown in figure 4, a correlation was found between stiffness and volume fraction determined via micro-CT. The exponential fit shows for the stiffness a factor 2.5 and for the strength a factor 2.1. These factors indicate, as was expected, that the pore shape of the assessed structures lies between what Gibson and Ashby[31] define as being an open cell and a honeycomb. Equation 1 shows the correlation between the stiffness of the porous structure and the volume fraction for open cells. Thus, if open cells would be assumed, from the fit for the stiffness it could be concluded that the stiffness of the bulk rapid prototyped material should be about 47 GPa (fig. 4). This was indeed confirmed through experimental mechanical testing, showing an E-modulus for the bulk rapid prototyped Ti6Al4V of about 42 GPa.

$$E = E_s * (vol.frac.)^2 \qquad \text{eq. 1}$$

where E is the stiffness of the porous structure and E_s the stiffness of the bulk material[31].

4. Conclusion

On one hand, the new micro-CT loading stage was proven to give accurate and correct results for the global mechanical properties of the tested rapid prototyped Ti6Al4V porous structures. On the other hand however, it was found that stepwise loading with intermediate micro-CT imaging induces errors in the stress-strain determination for these materials. It was also determined that there was no inter-batch variation for both morphological and mechanical properties. Thus, prior to stepwise loading, at least one sample of each batch should be loaded continuously. Finally, correlations between the morphology and the mechanical properties were made. The correlation functions can be applied to tailor the design according to the required stiffness and strength.

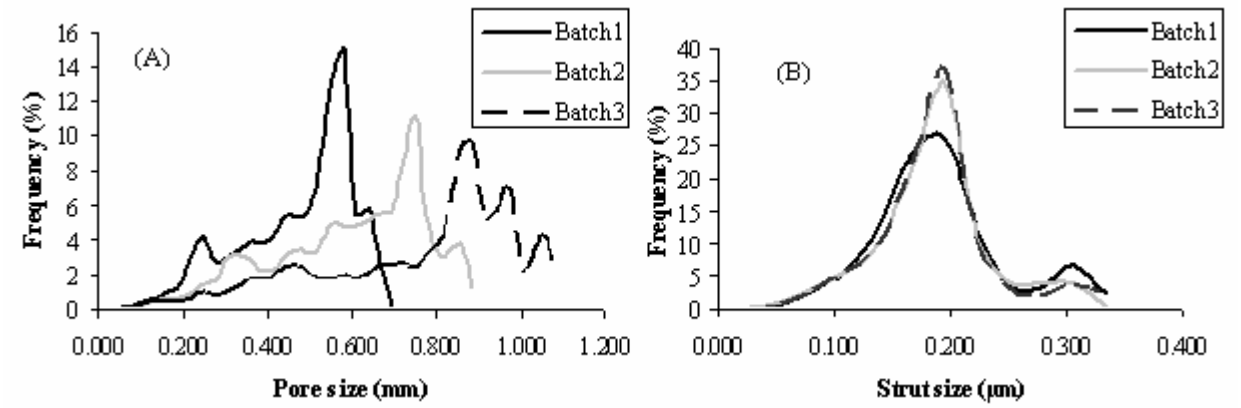

Figure 3. A) Pore size distribution for the three different designs and B) their strut size distribution. It can be seen that for the different designs indeed the strut size is kept constant, while the pore size is altered.

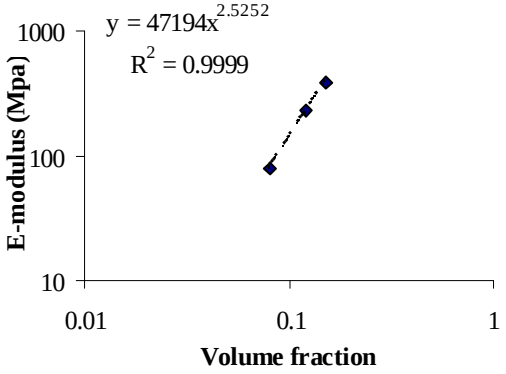

Figure 4. Correlation between the stiffness and the volume fraction of the samples, determined via micro-CT

5. References

[1] H. Bart-Smith et al., Compressive deformation and yielding mechanisms in cellular Al alloys determined using X-ray tomography and surface strain mapping, Acta Materialia 46 (10), 1998, P3583-3592.

[2] E. Maire et al., Recent results on 3D characterisation of microstructure and damage of metal matrix composites and a metallic foam using X-ray, Materials Science and Engineering a-Structural Materials Properties Microstructure and Processing 319 2001, P216-219.

[3] A. H. Benouali et al., Investigation on the influence of cell shape anisotropy on the mechanical performance of closed cell aluminium foams using micro-computed tomography, Journal of Materials Science 40 (22), 2005, P5801-5811.

[4] T. Dillard et al., 3D quantitative image analysis of open-cell nickel foams under tension and compression loading using X-ray microtomography, Philosophical Magazine 85 (19), 2005, P2147-2175.

[5] H. Toda et al., In-situ observation of fracture of aluminium foam using synchrotron X-ray microtomography, Advances in Fracture and Strength, Pts 1- 4 297-300 2005, P1189-1195.

[6] H. Toda et al., Quantitative assessment of microstructure and its effects on compression behavior of aluminum foams via high-resolution synchrotron X-ray tomography, Metallurgical and Materials Transactions a-Physical Metallurgy and Materials Science 37A (4), 2006, P1211-1219.

[7] T. Ohgaki et al., In situ observations of compressive behaviour of aluminium foams by local tomography using high-resolution X-rays, Philosophical Magazine 86 (28), 2006, P4417-4438.

[8] R. Müller et al., Micro-compression: a novel technique for the nondestructive assessment of local bone failure, Technology and Health Care 6 1998, P433-444.

[9] R. Muller et al., Micro-mechanical evaluation of bone microstructures under load, Proceedings of SPIE 4503 2002, P189-200.

[10] A. Nazarian et al., Time-lapsed microstructural imaging of bone failure behavior, Journal of Biomechanics 37 (1), 2004, P55-65.

[11] A. Nazarian et al., Design and implementation of a novel mechanical testing system for cellular solids, Journal of Biomedical Materials Research Part B-Applied Biomaterials 73B (2), 2005, P400-411.

[12] S. Nagaraja et al., Trabecular bone microdamage and microstructural stresses under uniaxial compression, Journal of Biomechanics 38 (4), 2005, P707-716.

[13] J. C. M. Teo et al., Relationship between CT intensity, micro-architecture and mechanical properties of porcine vertebral cancellous bone, Clinical Biomechanics 21 (3), 2006, P235-244.

[14] B. K. Bay et al., Digital volume correlation: Three-dimensional strain mapping using X-ray tomography, Experimental Mechanics 39 (3), 1999, P217-226.

[15] B. A. Roeder et al., Local, three-dimensional strain measurements within largely deformed extracellular matrix constructs, Journal of Biomechanical Engineering-Transactions of the Asme 126 (6), 2004, P699-708.

[16] T. S. Smith et al., Digital volume correlation including rotational degrees of freedom during minimization, Experimental Mechanics 42 (3), 2002, P272-278.

[17] Y. Wang et al., Full-field measurements of heterogeneous deformation patterns on polymeric foams using digital image correlation, International Journal of Solids and Structures 39 (13-14), 2002, P3777-3796.

[18] F. Snijkers et al., Porous Materials as Scaffold for Bone Replacement, Acers-meeting. 2005.

[19] S. Impens et al., Production and characterization of CaP en Ti scaffolds for bone tissue engineering, 19th European Conference on Biomaterials. 2005.

[20] K. F. Leong et al., Solid freeform fabrication of three-dimensional scaffolds for engineering replacement tissues and organs, Biomaterials 24 (13), 2003, P2363-2378.

[21] J. M. Williams et al., Bone tissue engineering using polycaprolactone scaffolds fabricated via selective laser sintering, Biomaterials 26 (23), 2005, P4817-4827.

[22] D. A. Hollander et al., Structural, mechanical and in vitro characterization of individually structured Ti-6Al-4V produced by direct laser forming, Biomaterials 27 (7), 2006, P955-963.

[23] L. A. Feldkamp et al., Practical Cone-Beam Algorithm, Journal of the Optical Society of America a-Optics Image Science and Vision 1 (6), 1984, P612-619.

[24] P. Ruegsegger et al., A microtomographic system for the nondestructive evaluation of bone architecture, Calcified Tissue International 58 (1), 1996, P24-29.

[25] A. Y. Sasov, Microtomography .1. Methods and Equipment, Journal of Microscopy-Oxford 147 1987, P169-178.

[26] G. Kerckhofs et al., Validation of x-ray microfocus computed tomography as an imaging tool for porous structures, Review of Scientific Instruments 79 (1), 2008.

[27] M. Ding et al., Age variations in the properties of human tibial trabecular bone, Journal of Bone and Joint Surgery-British Volume 79B (6), 1997, P995-1002.

[28] M. Ding et al., Accuracy of cancellous bone volume fraction measured by micro-CT scanning, Journal of Biomechanics 32 (3), 1999, P323-326.

[29] B. De Man et al., Metal streak artifacts in X-ray computed tomography: A simulation study, Ieee Transactions on Nuclear Science 46 (3), 1999, P691-696.

[30] B. De Man et al., Reduction of metal streak artifacts in x-ray computed tomography using a transmission maximum a posteriori algorithm, Ieee Transactions on Nuclear Science 47 (3), 2000, P977-981.

[31] L. J. Gibson et al., Cellular solids: structure and properties. 1988: Pergamon Press.